Large-Scale Growth of Two-Dimensional SnS_2 Crystals Driven by Screw Dislocations and Application to Photodetectors

Jing Xia, Dandan Zhu, Lei Wang, Ben Huang, Xing Huang, and Xiang-Min Meng**

2D SnS_2 crystals are attracting increasing attention owning to the huge potential for electronic and optoelectronic applications. However, batch production of 2D SnS_2 crystals via a simple vapor process remains challenging by far. Moreover, the growth mechanism for vapor growth of 2D SnS_2 is not well documented as well. Herein, a simple approach is presented for preparation of large-scale 2D SnS_2 crystals on mica sheets and it is demonstrated that these 2D crystals follow a screw-dislocation-driven (SDD) spiral growth process. The synthesized 2D crystals show hexagonal and truncated triangular shapes with the lateral size ranging from a few micrometers to dozens of micrometers. Observations of key features for screw dislocations, such as helical fringes, dislocation hillocks, and herringbone contours, solidly confirm the SDD spiral growth behavior of the SnS_2. Possible mechanism is proposed in this work to show the generation and propagation of screw dislocations. Furthermore, in order to explore the optoelectronic property of the SnS_2, photodetectors based on 2D SnS_2 crystals are fabricated. The resulting device shows excellent operating characteristics, including good photo-stability and reproducibility as well as a fast photoresponse time (≈42 ms), which enable the SnS_2 a promising candidate for photodetectors.

1. Introduction

2D layered metal dichalcogenides (MDCs) (YX_2; Y = Mo, Nb, Sn, Ga, etc.; X = S, Se, Te) are a big family composed of more than 40 members.[1–4] Among them, semiconducting MoS_2 has been the most widely studied one owning to its fascinating properties such as thickness-dependent bandgaps,[3,5] valley polarization,[6,7] piezoelectricity,[8,9] and valley Hall effect.[10,11] While MoS_2 has shown its great significance for fundamental research and various applications, other MDCs may provide important access to new physics or novel devices as well.[12–14]

Tin disulfide (SnS_2), one member of IV–VI MDCs, is also an important semiconductor with an indirect band gap of 2.2 eV.[15,16] With its earth abundant and environment friendly characters, SnS_2 has emerged as an important building block for sustainable electronic and optoelectronic applications. In particular, recent studies have demonstrated the enormous potential of 2D SnS_2 for applications in high-performance field effect transistors (FETs) and photodetectors.[17–19] For example, P. Sutter' group reported that FETs constructed from few-layer SnS_2 can exhibit a carrier mobility of about 5 $cm^2\ V^{-1}\ S^{-1}$ and a high on–off current ratio exceeding 10^7.[17] They further revealed that the carrier mobility can be markedly enhanced by fabricating solution-gated FETs, which promoted the carrier mobility up to 230 $cm^2\ V^{-1}\ S^{-1}$. Very recently, Su et al. demonstrated that SnS_2 nanoplate-based photodetectors had a fast photoresponse time as low as 5 μs, which is much lower than those from photodetectors made of GaSe, GaTe, GeSe, $MoSe_2$, and so on.[18,20–23] Furthermore, it has also been verified that heterostructures based on 2D SnS_2 crystals with other MDCs can offer diversified material platforms for electronic structure engineering of 2D semiconducting heterostructures and new device applications in electronics and optoelectronics.[15]

So far, several methods including exfoliation (chemical or physical),[16,17] chemical bath deposition,[24] solvothermal route,[25] sulfurization of tin dioxide,[18] and molecular beam epitaxy,[26] have been reported to prepare 2D SnS_2 crystals. However, exfoliation of bulk material lacks the controllability in uniformity, size, and thickness of the nanosheets, which unfits for large-scale device fabrication. Through preliminarily introducing nucleation sites on the SiO_2/Si substrates via lithography, Su et al. have reported the controlled synthesis of thin crystal arrays of SnS_2 using chemical vapor deposition.[18] Nevertheless, the utilization of lithography and metal seeds, such as Pd/Cr, Cr, and Ni, is not cost effective and can cause impurity in the synthesized SnS_2 nanoplates. Therefore, large-scale growth of 2D SnS_2 crystals via a simple and efficient approach is still needed. Besides, it is also worth mentioning that due to the limited reports on the synthesis of SnS_2, the underlying

J. Xia, D. D. Zhu, L. Wang, B. Huang, Prof. X.-M. Meng
Key Laboratory of Photochemical Conversion and Optoelectronic Materials
Technical Institute of Physics and Chemistry
Chinese Academy of Sciences
Beijing 100190, P. R. China
E-mail: mengxiangmin@mail.ipc.ac.cn
Dr. X. Huang
Inorganic Department
Fritz Haber Institute of Max Planck Society
Faradayweg 4-6, 14195 Berlin, Germany
E-mail: xinghuang0214@mail.ipc.ac.cn

DOI: 10.1002/adfm.201501495

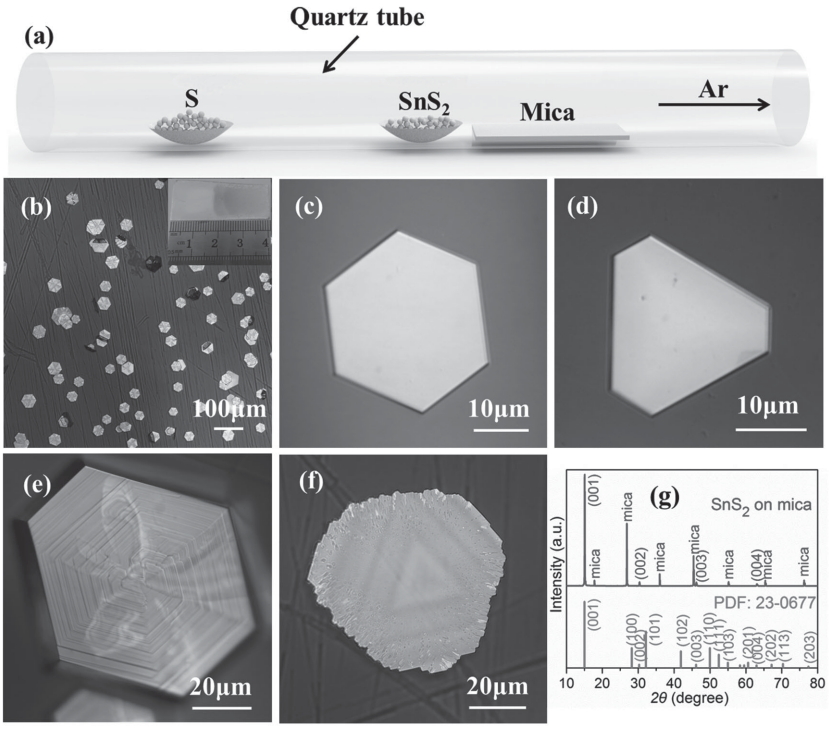

Figure 1. a) Schematic illustration for synthesizing 2D SnS_2 crystals. b) Optical image of large-scale 2D SnS_2 crystals. Inset shows the photograph of a mica substrate with the SnS_2 sample on its surface. c,d) Bright-field optical images of hexagonal and truncated triangular SnS_2 crystals, respectively. e,f) Bright-field optical images of two SnS_2 crystals showing spiral patterns and thin-film interference pattern, respectively. g) XRD pattern of the SnS_2 sample. The reference PDF data is also shown.

mechanism for vapor growth of 2D SnS_2 crystals remains unclear so far.

Here, using a simple atmospheric pressure vapor deposition (APVD) method, we successfully synthesize a large scale of 2D SnS_2 crystals on mica substrates. In addition to the large-size hexagonal SnS_2 crystals, truncated triangular crystals are also observed. Some key screw dislocation features, such as helical fringes, herringbone contours, and dislocation hillocks, are identified in the as-synthesized crystals, from which we conclude that the SnS_2 grows into 2D crystals through a screw-dislocation-driven (SDD) spiral growth mode. Relevant schematic models are used to illustrate the generation and propagation of screw dislocations during the growth. Finally, optoelectronic property of the 2D SnS_2 crystals is investigated by directly fabricating photodetectors on mica substrates. The device shows a fast response time of ≈42 ms, good photo-stability and reproducibility, suggesting that the 2D SnS_2 crystals could be an appealing material for optoelectronic devices.

2. Results and Discussion

We synthesized 2D SnS_2 crystals using an APCVD method, which is schematically illustrated in **Figure 1**a. Briefly, SnS_2 powder was utilized as the source material and was put at the center of the heating zone. Several pieces of mica sheets were loaded at the downstream of tube and served as the substrates for growth of SnS_2. Additionally, in order to inhibit the disproportionation of SnS_2 into SnS phase,[27] S powder was also used in our synthesis and placed at the upstream of the SnS_2 powder. Eventually, SnS_2 crystals can be achieved on substrates through heating SnS_2 powder to 700 °C. More details can be found in the Experimental Section.

Figure 1b shows a typical optical microscopy (OM) image of the as-prepared 2D SnS_2 crystals grown on a mica substrate. It can be seen that the majority of the 2D SnS_2 crystals show a hexagonal shape with the lateral size ranging from 13 to 43 μm. Additionally, SnS_2 crystals with truncated triangular shape were also obtained, as shown in Figure 1d. The spatial distribution of these 2D crystals suggests that SnS_2 randomly nucleated on mica substrates, rather than position-controlled alignment. Although the synthesized crystals lack uniformity in location and crystal size, the mica substrate has a ≈3 cm^2 region containing hundreds of isolated 2D crystals (inset in Figure 1b), which is enough for future large-scale device fabrication. Figure 1c displays an enlarged OM image of a hexagonal SnS_2 crystal with the lateral size of ≈15 μm. From a macroscopic perspective, the uniform color contrast of this crystal indicates that it has a relative smooth surface. However, the AFM characterization performed later demonstrates that the surface is in fact not atomically smooth. Instead, it shows a clear dislocation hillock consisting of several spiral patterns on the surface (**Figure 2**b). Figure 1e shows another type of SnS_2 crystal we achieved. Unlike the crystal exhibited in Figure 1c, this type of SnS_2 generally has clear spiral patterns on surface, which is due to the bunched steps in spiral structures as evidenced by AFM measurement (Figure 2d). On the basis of those evidences, we believe that the screw dislocations exist in the synthesized 2D SnS_2 crystals. Another obvious sign for the existence of screw dislocations is shown in Figure 1f. As can be seen, the thin-film interference pattern in triangular rings was generated between the surface of 2D crystal and the reflective mica substrate under bright-filed optical microscopy. The regular color change of the pattern in fact reflects a geometry and thickness variation of the crystal surface. Similar phenomenon has been reported by Jin's group on the nanoplate of zinc hydroxyl sulfate driven by screw dislocations.[28] According to their study, this type of nanoplate contains a dislocation hillock on the surface. Because of this hillock, the flake indeed has a pyramid-like morphology. In short, these preliminary results suggest the existence of screw dislocations in the synthesized 2D SnS_2 crystals.

To investigate the phase structure of the SnS_2 sample, X-ray diffraction (XRD) measurement was carried out, and the result is exhibited in Figure 1g. As indicated, the SnS_2 crystals have a 2T-type hexagonal structure with lattice constants of $a = b =$ 0.3645 nm, $c = 0.589$ nm (JCPDS PDF number 23-0677).[16,29,30] The sole strong diffraction reflection located at 15° can be

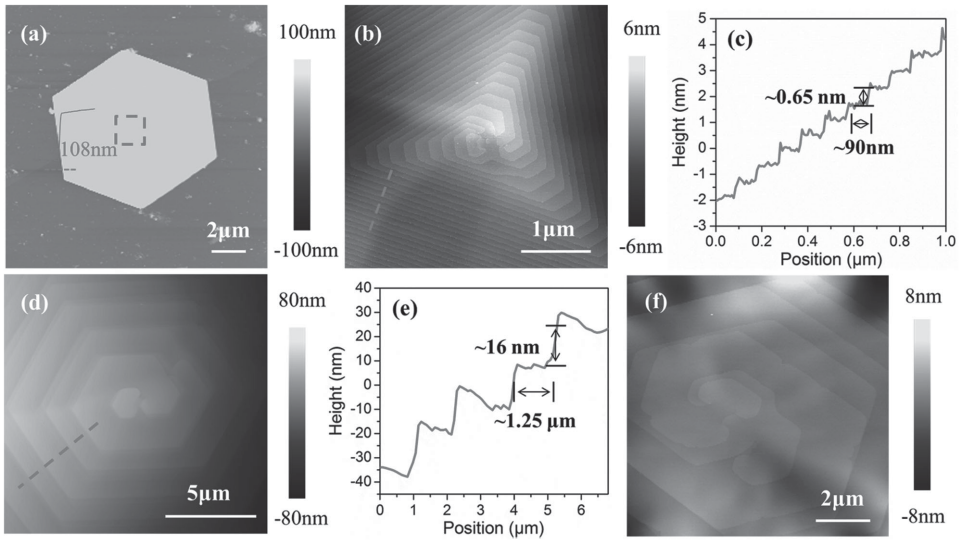

Figure 2. a) AFM image and height profile of a hexagonal SnS_2 crystal. b) AFM image of the central region marked by a dashed square in (a). The dislocation hillock and terraces can be clearly found. c) Height profile of the hillock along the dashed line in (b). d) AFM image of the central region of a thick crystal showing hexagonal spiral fringes. e) Height profile of the flake along the dashed line in (d). f) AFM image of the central region of another flake showing two spiral fringes with counterclockwise rotation direction.

indexed to the (0001) plane of SnS_2, while those small diffraction reflections at about 30.3°, 46.1°, 62.9° can be assigned to the (0002), (0003), and (0004) planes, respectively. The dominance of (000*N*) (*N* = 0, 1, 2, etc.) peaks strongly suggests that the 2D SnS_2 crystals grow preferably along the *Z*-direction with (0001) plane as the basal plane. Raman characterization was also performed on the SnS_2 crystals using a 532 nm laser for excitation, as displayed in Figure S1 (Supporting Information). As seen, there are two typical Raman active modes appeared in the spectrum, i.e., a strong A_{1g} Raman mode at 313.9 cm^{-1} and a weak E_g Raman mode at 202.2 cm^{-1}, which further confirm that these crystals are SnS_2.[17–19]

We also performed AFM measurement on the 2D crystals to probe their surface features in detail. Shown in Figure 2a is the AFM image of a hexagonal SnS_2 crystal with a thickness of ≈108 nm. The central region (dashed square in Figure 2a) of this crystal is displayed in Figure 2b, in which dislocation hillock composed of seven spiral patterns in clockwise direction can be clearly observed. This result strongly manifests that the surfaces of the 2D SnS_2 crystals (Figure 1c,d) are not atomically flat. Instead, they show a pyramid-like structure with an extremely large width-to-thickness ratio. Figure 2c shows the height profile along the dashed line in Figure 2b. The step height of hillock is measured to be ≈0.65 nm, close to the thickness of a SnS_2 monolayer (0.59 nm) and a length of one unit Burgers vector.[16,17] Together with the AFM image in Figure 2b, we learn that the hillock is generated by one dislocation with seven elementary Burgers vectors.[31–33] In addition, the hillock resulting from a single dislocation with a much larger Burgers vector was also observed, as shown in Figure 2d. Interestingly, instead of showing well-separated steps (Figure 2b), the hillock of the crystal in Figure 2d displays bunched steps. This is presumably due to the similarity in advancing speed of each layer in the screw dislocation.[34,35] According to the height profile exhibited in Figure 2e, the step height is about 16 nm, equal to a thickness of 27 monolayers and a Burgers vector of 27 (16 nm/0.59 nm ≈27). With such large Burgers vector and bunched steps, the visibility of the dislocation spirals can be increased greatly. Based on the above results, we can conclude that the SnS_2 crystals follow a SDD spiral growth mode. On the other hand, it is also worth mentioning that the spiral patterns on 2D SnS_2 crystals are not necessary to be clockwise (Figure 2b,d and Figure S2a, Supporting Information), counterclockwise spiral patterns are also identifiable, as shown in Figure 2f and Figure S2b (Supporting Information).

In order to examine the microscopic structure of the 2D SnS_2 crystals, transmission electron microscopy (TEM) and electron diffraction technique were then utilized. **Figure 3**a shows a bright-field (BF) TEM image of a 2D SnS_2 crystal. Appearance of a terrace in the bottom left corner of the hexagonal crystal indicates that this crystal was possibly following a SDD growth mode. The high-resolution TEM (HRTEM) image (from the region labeled by a circle in Figure 3a) clearly exhibits a direct view of hexagonal lattice structure, in good agreement with the atomic mode of SnS_2 with a hexagonal arrangement of Sn and S atoms (inset in Figure 3b). The lattice fringes measured from the HRTEM image is about 0.32 nm, which fits well to the *d*-spacing of {10–10} planes.[16] Figure 3c shows the selected-area electron diffraction (SAED) pattern recorded from the circle region of the crystal in Figure 3a. The well-arranged diffraction spots with a sixfold symmetry confirm the good quality and the single crystallinity of this crystal. Together with the HRTEM characterization, it can be concluded that the 2D hexagonal crystal is enclosed with {10–10} facets and results from a fast laterally growth of <2–1–10> and a slow vertically growth of the [0001] direction. Figure 3d exhibits a BF TEM image of a SnS_2 crystal, in which the herringbone contours can be clearly observed (indicated by arrows). Moreover, spiral

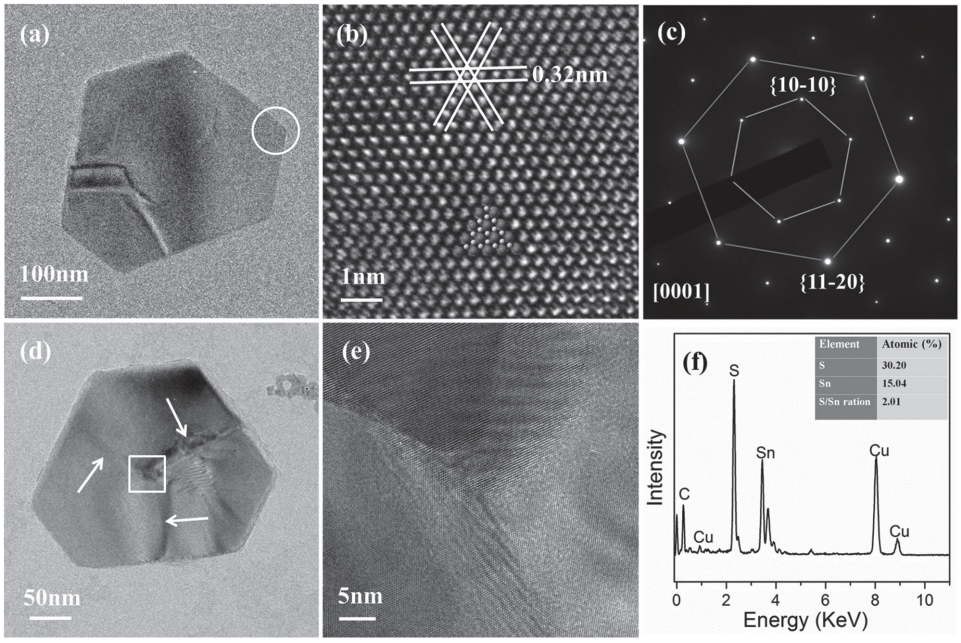

Figure 3. a) Bright-field TEM image of a SnS_2 crystal with a terrace appeared in the bottom left corner of the crystal. b) HRTEM image obtained from the region labeled with a circle in (a). Inset exhibits an atomic model of Sn and S atoms. c) The corresponding SAED pattern. d) Bright-field TEM image of a SnS_2 crystal showing the herringbone contours (indicated by arrows) on the surface. e) HRTEM image of the center region marked by a square in (d). f) EDX spectrum of the SnS_2 crystal. Inset shows the ratio of Sn and S atoms.

arms initiated from the dislocation core can also be identified from the central region of the crystal, as exhibited in Figure 3e. More TEM images of SnS_2 with spiral structures can be found in Figure S3 (Supporting Information). In short, those results solidly demonstrate the existence of screw dislocations in the synthesized SnS_2 crystals, in line with our optical observation and AFM characterization. The energy-dispersive X-ray spectroscopy (EDX) was also adopted to study the composition of the crystals. As shown in Figure 3f, in addition to the C and Cu elements that are from the TEM grid, the spectrum only shows signals of S and Sn with an atomic ratio of ≈2:1, signifying a high purity of the synthesized SnS_2 crystals.

SDD growth has been demonstrated to be a universal mechanism for growth of 1D and 2D nanocrystals, which prefers to occur when the supersaturation of system is relatively low.[28,31,32,36–41] Considering that only a small amount of SnS_2 powder was used in our synthesis, it is quite logical that the as-prepared 2D SnS_2 crystals followed a SDD growth mode as we evidenced. However, unlike SDD growth of 2D MoS_2 and WSe_2 which shows a screw dislocation with one or two unit Burger vectors,[31,39] 2D crystals in our study often show a screw dislocation with a very large Burger vector, as the cases exhibited in Figure 2b,d. The reason is not clear to us, which is probably related to the growth kinetics dependent on environmental condition utilized. Very recently, screw dislocations introduction mechanisms have been proposed and discussed in the CVD growth of 2D materials.[28,31,32,39] For instance, during the spiral growth of MoS_2, Zhang et al. believed that screw dislocation can be generated through an accidental overgrowth of two exposed edges at the initial stage due to the formation of large amount of MoO_{3-x} within a short time, which leads to a slipped edge as a screw defect.[39] In contrast, Huang et al. suggested that the screw dislocation in WSe_2 flake can be created by intersection of two WSe_2 domains at initial stage.[31] Unfortunately, the mechanisms aforementioned are unadaptable to our object considering the differences in experimental condition and the result we characterized. In the present study, the screw dislocations seem to be introduced directly on the planar surface of 2D SnS_2 (Figure 3a and Figure S3, Supporting Information) rather than a result of accidental overgrowth of two exposed edges or intersection of two domains. Alternately, it is also known that imperfect nucleation on crystal surfaces is a common way for production of screw dislocations.[41–43] Given the reactions occurred in the present experiment, we consider that the imperfect nucleation caused by impurity inclusion in the gaseous species is the most likely reason for screw dislocation introduction. As stated above, we used SnS_2 and S powder as the source materials for the growth of 2D SnS_2 crystals. Ideally, SnS_2 powder will first thermally evaporate under high-temperature condition. Then, the resulting gaseous species nucleate on the substrates and grow up to 2D SnS_2 crystals. However, the possible disproportionation of SnS_2 could lead to the formation of some intermediate SnS species which may escape from the sulfidation and nucleated on the preformed SnS_2 grains.[27] Owing to the structural incompatibility of SnS and SnS_2,[44,45] the impurity inclusion in gaseous species may result in an imperfect nucleation on the SnS_2 planar surface and the generation of a terrace as a screw defect (Figure 3a and **Figure 4**a). According to Burton–Cabrera–Frank (BCF) theory,[34] once the screw dislocation is created, the crystal growth at the edge of the dislocation is energetically favorable, which will result in a spiral growth of the crystal (Figure 4b–d). Due to the existence

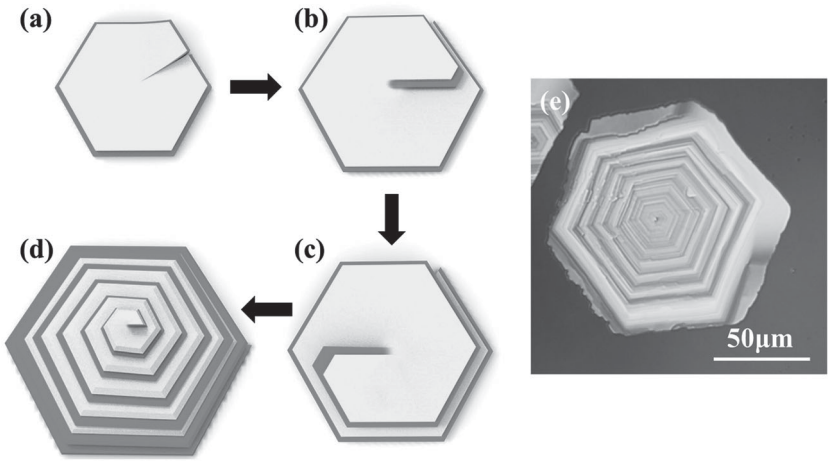

Figure 4. a–d) Schematic modes showing the growth process of a spiraled SnS_2 crystal. e) Optical image of a typical SnS_2 crystal with hexagonal spiral patterns on its surface.

of high strain in the dislocation core, the growth rate normal to the surface is very slow compared to the lateral growth rate; thus, the crystal almost expends laterally.[31,39] The final pyramid shape of the 2D SnS_2 crystals is because that the bottom layers are formed earlier and have more time to grow with respect to the top layers, as shown in Figure 4d,e.[28,39] We believe that by optimizing the experimental parameters, the SDD growth can also occur on other 2D MDCs.

The optoelectronic properties of the 2D SnS_2 crystals were also investigated, as shown in **Figure 5**. Figure 5a illustrates the schematic diagram of a SnS_2 photodetector. The device was constructed directly on the mica substrate with Au as electrodes, which was later annealed at 200 °C in an Ar atmosphere to reduce resistance. The detailed fabrication process can be found in the Experimental Section. Figure 5b shows the current (I)–voltage (V) characteristics of the photodetector in dark and in the presence of laser illumination with different light intensities. The I–V plots show a linear increase of the current with the applied voltage ranging from –10 to 10 V, indicating a good contact between the SnS_2 and Au electrodes.[46] In contrast to the dark current, a pronounced increase in photocurrent ($I_{ph} = I_{illuminated} - I_{dark}$) was observed when the device was illuminated by the laser, suggesting a strong photoresponse of the device. In Figure 5c, the photocurrent as a function of the light intensity was plotted with stars. By fitting the experimental data, it is found that the photocurrent can be expressed by a power-law equation $I_{ph} \propto P^{0.6}$, where P is the light intensity.[23,47] The deviation from the ideal slope may be attributed to the dislocation defects in the SnS_2 crystals. One critical parameter for estimating the performance of the photodetector is the photoresponsivity ($R\lambda$), which can be given by $R\lambda = I_{ph}/PS$, where S is the effective area of the photodetector.[48] For our device, the effective exposure area is about 120 μm^2. With a bias voltage of 10 V, the photoresponsivity can be expressed as $R\lambda = I_{ph}/PS = P^{0.6}/PS = P^{-0.4}/S$. Considering that the light intensity is ranging from 1 and 100 mW cm^{-2}, the photoresponsivity is calculated to be 2–0.31 A W^{-1}, which are comparable to those of the photodetectors based on graphene and $MoSe_2$.[20,49]

Another important parameter that should be considered for evaluating the performance of the photodetector is the response time. To test this, we measured the time-resolved photoresponse of the device by switching the laser on and off periodically, as shown in Figure 5d. The regular changes of the plot indicate that the device has a repeatable and stable response to the light illumination. The dark current of the device is relatively large, which is most likely due to a large number of free charges caused by the dislocation defects. Figure 5e,f shows the rise and decay behaviors of the current. When the light illumination was turned on, the current increased by more than 90% in 42 ms and then rose with a little slower kinetics. Meanwhile, the current reduced dramatically by more than 90% in 42 ms after the laser was turned off. According to the definition of response time,[48,50] we conclude that the rise and decay times are about 42 ms, which are much faster than those of so far reported photodetectors based on In_2Se_3,[51] tellurium nanoplates,[50] and so on. The excellent photoresponse properties of the device, such as good photo-stability and reproducibility, and fast response time, enable the 2D SnS_2 crystals to be a promising building block for high-performance optoelectronic devices.

3. Conclusion

In summary, we report the growth of large-scale 2D SnS_2 crystals on mica substrates using a simple APVD method for the first time. The typical products show hexagonal and truncated triangular shapes with the lateral size ranging from a few micrometers to dozens of micrometers. Detailed characterizations reveal that the synthesized 2D SnS_2 crystals follow a SDD spiral growth fashion. Evidences for this growth mode include spiral fringes, herringbone contours, and dislocation hillocks. Schematic diagrams were used to illustrate the formation and propagation of the screw dislocations. Moreover, photodetectors based on the as-grown 2D SnS_2 crystals were directly fabricated on mica substrates and the resulting device showed a fast response time ≈42 ms, good photo-stability and reproducibility, making it an appealing material for optoelectronic devices.

4. Experimental Section

Synthesis: To synthesize 2D SnS_2 crystals, an APVD method was adopted. The reaction took place in a high-temperature tube furnace. In a typical growth, a small amount of SnS_2 powder was put in a ceramic boat at the center of the heating zone, and 1 g of S powder was put in another ceramic boat at the upstream with a distance of about 18 cm. Newly cleaved mica substrates were placed downstream to the center at a distance of about 5–15 cm. The furnace chamber was pumped down to expel the air and then filled with high-purity Ar to atmospheric pressure. Next, the center of heating zone was heated to 700 °C within 35 min. When the furnace reached 700 °C, the temperature of the S powder at the upstream was about 300 °C. The furnace was kept at 700 °C for

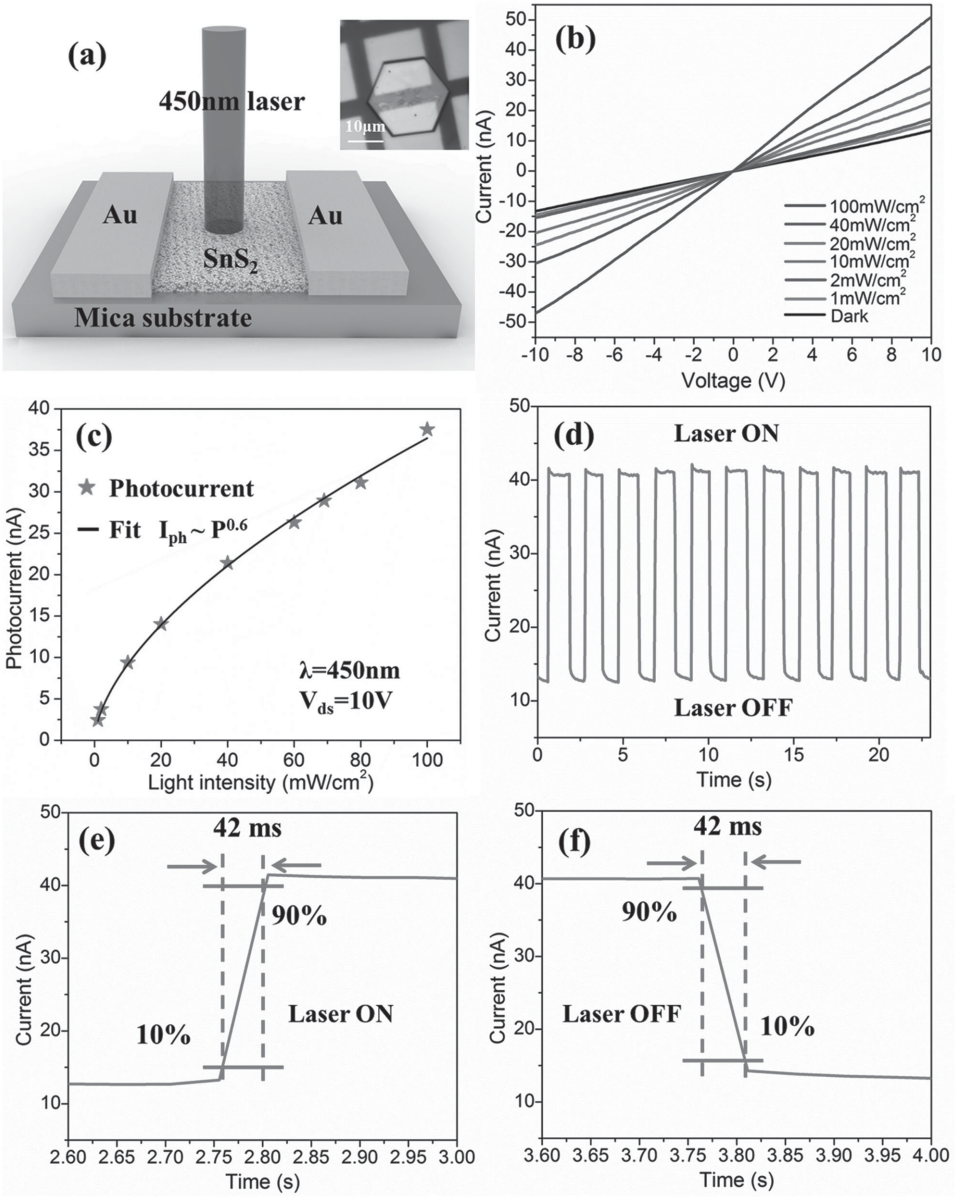

Figure 5. a) Schematic view of a SnS_2 photodetector with 450 nm laser for illumination. Inset shows the optical image of a 2D SnS_2 crystal-based photodetector. b) *I–V* characteristics of the device in the dark and in the presence of the laser illumination with different light intensities. c) The light intensity dependence of the photocurrent under the bias voltage of 10 V. d) The time-resolved photoresponse of the device at the bias voltage of 10 V and light intensity of 80 mW cm^{-2}. e,f) Enlarged portions of a 2.6–3 s range and a 3.6–4 s range, respectively.

15 min before being allowed to room temperature naturally. During the growth process, high-purity Ar with a flow rate of 80 sccm was used as the gas carrier.

Characterization: Optical images were obtained using an optical microscope (Nikon Inverted Microscope Eclipse Ti-U with a CCD of Nikon Digital Sight). X-ray diffraction pattern of the sample was recorded using a Bruker D 8 Focus powder X-ray diffractometer using Cu Kα radiation (λ = 1.5418 Å). Raman spectra and mappings were taken in the Renishaw InVia Raman Microscope and Nanophoton Raman 11 Microscope, respectively. AFM characterization was taken by an atomic force microscope of Bruker Mutimode 8. The structure and composition of the sample were investigated using JEOL JEM-2100F equipped with an energy-dispersive X-ray spectroscopy.

Device Fabrication and Measurements: The photodetectors based on 2D SnS_2 crystals were directly fabricated on mica substrates. Au electrodes were deposited using a copper grid shadow mask. The devices with a gap of 7 μm were annealed at 200 °C for 2 h in an Ar atmosphere to reduce resistance. Photoelectric measurements were performed using a Lakeshore probe station and a Keithley-4200 SCS semiconductor parameter analyzer under atmosphere environment. A 450 nm laser was used as the light source. A laser attenuator was used to adjust the intensity of the incident beam, which was measured by a laser power meter.

Supporting Information

Supporting Information is available from the Wiley Online Library or from the author.

Acknowledgements

The authors thank the financial supports from the "Strategic Priority Research Program" of Chinese Academy of Sciences (Grant No. XDA09040203), and 973 Project (2012CB932401).

Received: April 14, 2015
Revised: May 7, 2015
Published online: June 1, 2015

[1] S. Z. Butler, S. M. Hollen, L. Y. Cao, Y. Cui, J. A. Gupta, H. R. Gutierrez, T. F. Heinz, S. S. Hong, J. X. Huang, A. F. Ismach, E. Johnston-Halperin, M. Kuno, V. V. Plashnitsa, R. D. Robinson, R. S. Ruoff, S. Salahuddin, J. Shan, L. Shi, M. G. Spencer, M. Terrones, W. Windl, J. E. Goldberger, *ACS Nano* **2013**, *7*, 4.

[2] M. Xu, T. Liang, M. Shi, H. Chen, *Chem. Rev.* **2013**, *113*, 5.

[3] Q. H. Wang, K. Kalantar-Zadeh, A. Kis, J. N. Coleman, M. S. Strano, *Nat. Nanotechnol.* **2012**, *7*, 11.

[4] J. N. Coleman, M. Lotya, A. O'Neill, S. D. Bergin, P. J. King, U. Khan, K. Young, A. Gaucher, S. De, R. J. Smith, I. V. Shvets, S. K. Arora, G. Stanton, H.-Y. Kim, K. Lee, G. T. Kim, G. S. Duesberg, T. Hallam, J. J. Boland, J. J. Wang, J. F. Donegan, J. C. Grunlan, G. Moriarty, A. Shmeliov, R. J. Nicholls, J. M. Perkins, E. M. Grieveson, K. Theuwissen, D. W. McComb, P. D. Nellist, V. Nicolosi, *Science* **2011**, *331*, 6017.

[5] W. S. Yun, S. W. Han, S. C. Hong, I. G. Kim, J. D. Lee, *Phys. Rev. B: Condens. Matter* **2012**, *85*, 3.

[6] H. L. Zeng, J. F. Dai, W. Yao, D. Xiao, X. D. Cui, *Nat. Nanotechnol.* **2012**, *7*, 8.

[7] K. F. Mak, K. L. He, J. Shan, T. F. Heinz, *Nat. Nanotechnol.* **2012**, *7*, 8.

[8] H. Y. Zhu, Y. Wang, J. Xiao, M. Liu, S. M. Xiong, Z. J. Wong, Z. L. Ye, Y. Ye, X. B. Yin, X. Zhang, *Nat. Nanotechnol.* **2015**, *10*, 2.

[9] W. Z. Wu, L. Wang, Y. L. Li, F. Zhang, L. Lin, S. M. Niu, D. Chenet, X. Zhang, Y. F. Hao, T. F. Heinz, J. Hone, Z. L. Wang, *Nature* **2014**, *514*, 7523.

[10] K. F. Mak, K. L. McGill, J. Park, P. L. McEuen, *Science* **2014**, *344*, 6191.

[11] M. Tahir, A. Manchon, U. Schwingenschlogl, *Phys. Rev. B: Condens. Matter* **2014**, *90*, 12.

[12] M. Langer, M. Kisiel, R. Pawlak, F. Pellegrini, G. E. Santoro, R. Buzio, A. Gerbi, G. Balakrishnan, A. Baratoff, E. Tosatti, E. Meyer, *Nat. Mater.* **2014**, *13*, 2.

[13] S. Tongay, H. Sahin, C. Ko, A. Luce, W. Fan, K. Liu, J. Zhou, Y. S. Huang, C. H. Ho, J. Y. Yan, D. F. Ogletree, S. Aloni, J. Ji, S. S. Li, J. B. Li, F. M. Peeters, J. Q. Wu, *Nat. Commun.* **2014**, *5*, 3252.

[14] K. Xu, P. Z. Chen, X. L. Li, C. Z. Wu, Y. Q. Guo, J. Y. Zhao, X. J. Wu, Y. Xie, *Angew. Chem. Int. Ed.* **2013**, *52*, 40.

[15] X. W. Zhang, F. Meng, J. R. Christianson, C. Arroyo-Torres, M. A. Lukowski, D. Liang, J. R. Schmidt, S. Jin, *Nano Lett.* **2014**, *14*, 6.

[16] Y. F. Sun, H. Cheng, S. Gao, Z. H. Sun, Q. H. Liu, Q. Liu, F. C. Lei, T. Yao, J. F. He, S. Q. Wei, Y. Xie, *Angew. Chem. Int. Ed.* **2012**, *51*, 35.

[17] Y. Huang, E. Sutter, J. T. Sadowski, M. Cotlet, O. L. A. Monti, D. A. Racke, M. R. Neupane, D. Wickramaratne, R. K. Lake, B. A. Parkinson, P. Sutter, *ACS Nano* **2014**, *8*, 10.

[18] G. X. Su, V. G. Hadjiev, P. E. Loya, J. Zhang, S. D. Lei, S. Maharjan, P. Dong, P. M. Ajayan, J. Lou, H. B. Peng, *Nano Lett.* **2015**, *15*, 1.

[19] H. S. Song, S. L. Li, L. Gao, Y. Xu, K. Ueno, J. Tang, Y. B. Cheng, K. Tsukagoshi, *Nanoscale* **2013**, *5*, 20.

[20] J. Xia, X. Huang, L. Z. Liu, M. Wang, L. Wang, B. Huang, D. D. Zhu, J. J. Li, C. Z. Gu, X. M. Meng, *Nanoscale* **2014**, *6*, 15.

[21] D. J. Xue, J. H. Tan, J. S. Hu, W. P. Hu, Y. G. Guo, L. J. Wan, *Adv. Mater.* **2012**, *24*, 33.

[22] M. Mahjouri-Samani, R. Gresback, M. Tian, K. Wang, A. A. Puretzky, C. M. Rouleau, G. Eres, I. N. Ivanov, K. Xiao, M. A. McGuire, G. Duscher, D. B. Geohegan, *Adv. Funct. Mater.* **2014**, *24*, 40.

[23] F. C. Liu, H. Shimotani, H. Shang, T. Kanagasekaran, V. Zolyomi, N. Drummond, V. I. Fal'ko, K. Tanigaki, *ACS Nano* **2014**, *8*, 1.

[24] S. A. Liu, X. M. Yin, Q. Y. Hao, M. Zhang, L. M. Li, L. B. Chen, Q. H. Li, Y. G. Wang, T. H. Wang, *Mater. Lett.* **2010**, *64*, 21.

[25] Y. Zhang, P. Zhu, L. Huang, J. Xie, S. Zhang, G. Cao, X. Zhao, *Adv. Funct. Mater.* **2015**, *25*, 3.

[26] R. Schlaf, D. Louder, O. Lang, C. Pettenkofer, W. Jaegermann, K. W. Nebesny, P. A. Lee, B. A. Parkinson, N. R. Armstrong, *J. Vac. Sci. Technol. A* **1995**, *13*, 3.

[27] T. Shimada, F. S. Ohuchi, B. A. Parkinson, *J. Vac. Sci. Technol. A* **1992**, *10*, 3.

[28] S. A. Morin, A. Forticaux, M. J. Bierman, S. Jin, *Nano Lett.* **2011**, *11*, 10.

[29] Y. P. Du, Z. Y. Yin, X. H. Rui, Z. Y. Zeng, X. J. Wu, J. Q. Liu, Y. Y. Zhu, J. X. Zhu, X. Huang, Q. Y. Yan, H. Zhang, *Nanoscale* **2013**, *5*, 4.

[30] D. De, J. Manongdo, S. See, V. Zhang, A. Guloy, H. B. Peng, *Nanotechnology* **2013**, *24*, 2.

[31] L. Chen, B. L. Liu, A. N. Abbas, Y. Q. Ma, X. Fang, Y. H. Liu, C. W. Zhou, *ACS Nano* **2014**, *8*, 11.

[32] A. Zhuang, J. J. Li, Y. C. Wang, X. Wen, Y. Lin, B. Xiang, X. P. Wang, J. Zeng, *Angew. Chem. Int. Ed.* **2014**, *53*, 25.

[33] H. H. Teng, P. M. Dove, J. J. De Yoreo, *Geochim. Cosmochim. Acta* **2000**, *64*, 13.

[34] W. K. Burton, N. Cabrera, F. C. Frank, *Philos. Trans. R. Soc. London, A* **1951**, *243*, 866.

[35] R. Singh, S. B. Samanta, A. V. Narlikar, G. C. Trigunayat, *J. Cryst. Growth* **2000**, *213*, 1.

[36] F. Meng, S. A. Morin, A. Forticaux, S. Jin, *Acc. Chem. Res.* **2013**, *46*, 7.

[37] S. Jin, M. J. Bierman, S. A. Morin, *J. Phys. Chem. Lett.* **2010**, *1*, 9.

[38] S. A. Morin, S. Jin, *Nano Lett.* **2010**, *10*, 9.

[39] L. M. Zhang, K. H. Liu, A. B. Wong, J. Kim, X. P. Hong, C. Liu, T. Cao, S. G. Louie, F. Wang, P. D. Yang, *Nano Lett.* **2014**, *14*, 11.

[40] S. A. Morin, M. J. Bierman, J. Tong, S. Jin, *Science* **2010**, *328*, 5977.

[41] R. L. Penn, J. F. Banfield, *Science* **1998**, *281*, 5379.

[42] D. Kuhlmannwilsdorf, D. Pandey, P. Krishna, *Philos. Mag. A* **1980**, *42*, 4.

[43] D. Pandey, A. Baronnet, P. Krishna, *Phys. Chem. Minerals* **1982**, *8*, 6.

[44] T. Zhou, W. K. Pang, C. Zhang, J. Yang, Z. Chen, H. K. Liu, Z. Guo, *ACS Nano* **2014**, *8*, 8.

[45] G. Radovsky, R. Popovitz-Biro, M. Staiger, K. Gartsman, C. Thomsen, T. Lorenz, G. Seifert, R. Tenne, *Angew. Chem. Int. Ed.* **2011**, *50*, 51.

[46] O. Lopez-Sanchez, D. Lembke, M. Kayci, A. Radenovic, A. Kis, *Nat. Nanotechnol.* **2013**, *8*, 7.

[47] N. Perea-Lopez, A. L. Elias, A. Berkdemir, A. Castro-Beltran, H. R. Gutierrez, S. Feng, R. Lv, T. Hayashi, F. Lopez-Urias, S. Ghosh, B. Muchharla, S. Talapatra, H. Terrones, M. Terrones, *Adv. Funct. Mater.* **2013**, *23*, 44.

[48] P. A. Hu, Z. Z. Wen, L. F. Wang, P. H. Tan, K. Xiao, *ACS Nano* **2012**, *6*, 7.

[49] F. Xia, T. Mueller, Y.-m. Lin, A. Valdes-Garcia, P. Avouris, *Nat. Nanotechnol.* **2009**, *4*, 12.

[50] Q. S. Wang, M. Safdar, K. Xu, M. Mirza, Z. X. Wang, J. He, *ACS Nano* **2014**, *8*, 7.

[51] T. Zhai, X. Fang, M. Liao, X. Xu, L. Li, B. Liu, Y. Koide, Y. Ma, J. Yao, Y. Bando, D. Golberg, *ACS Nano* **2010**, *4*, 3.